Gold Bulletin (2020) 53:55–62
https://doi.org/10.1007/s13404-020-00274-1

ORIGINAL PAPER

Synthesis of amphiphilic Janus gold nanoparticles stabilized with triphenylphosphine and D-penicillamine by ligand exchange at toluene/water emulsion interface

Degui Li[2,3] · Yujia Luo[4] · Jiaxin Lan[3] · Zhihong Luo[3] · Fujie Li[3] · Kun Luo[1]

Received: 3 February 2020 / Accepted: 6 March 2020 / Published online: 14 March 2020

Abstract

Ligand exchange was triggered at toluene/water emulsion interface between homogeneous gold nanoparticles (Au NPs) with triphenylphosphine (PPh_3) and D-penicillamine (D-PA), resulted in amphiphilic Janus Au NPs with both phosphine and thiolate ligands. TEM and XRD analyses indicate that the product is composed of Au nanocrystals in an average diameter of about 3.7 nm. XPS, FTIR, Raman, and ^1H NMR analyses demonstrate that the Au NPs are protected with hydrophilic D-PA molecules and lipophilic PPh_3 ligands in a molecular ratio of ca. 1.8. The NOESY analysis and contact angle measurement further suggest that the D-PA and PPh_3 molecules are spontaneously separated to form compartmentalized hydrophilic and lipophilic regions on the individual Au NPs, which exhibit good catalytic performance and recyclability on the reduction of 4-nitrophenol. The results demonstrate that amphiphilic Janus Au NPs can be synthesized by partly exchange of PPh_3 with D-PA at toluene/water emulsion interface and are potentially applicable for other phosphine/thiolate pairs to modify Au NPs.

Keywords Janus · Amphiphilic · Gold nanoparticle · Ligand exchange · Toluene/water interface

Introduction

Since De Gennes coined the concept of Janus particle [1], enormous efforts have been devoted to the novel kind of colloids [2]. As a subcategory, amphiphilic Janus gold nanoparticle (Au NP) possesses a compartmentalized shell of two or more capping molecules with different affinity to oil and water phases [3, 4], which makes it behave like a "solid surfactant" to a large extent. Combining with the excellent chemical stability, biocompatibility, and catalytic activity of Au NPs [5, 6], the amphiphilic Janus Au NPs are expected to serve as novel heterogeneous catalysts [7, 8], sensors [9], and targeting drug carriers [10–13].

The well-defined segregation of capping ligands on Au NPs involves in delicate surface/interface engineering [14, 15]. Ligand exchange reaction at immiscible liquid/liquid interfaces is a straightforward approach, where a hydrophobic molecule dissolved in oil phase can be used to partly replace the original hydrophilic capping ligand on the precursor homogeneous Au NPs and vice versa, leading to amphiphilic Janus Au NPs. Alternatively, the Janus modification can be performed in one step, where the formation of Au NPs occurs at the interface with the bilateral supply of a hydrophobic ligand in oil and a hydrophilic molecule in water [16]. The spontaneous phase separation of capping molecules on Au NPs' surface was also reported to produce Janus Au NPs [17]. Among these methods, ligand exchange reaction is frequently used for its facile operation and flexible applicability.

S-, P-, N-, Si-, or Se-containing molecules are frequently selected as the capping ligands to stabilize Au NPs, owing to the strong bonding of the elements with Au atom. Rao et al.

Electronic supplementary material The online version of this article (https://doi.org/10.1007/s13404-020-00274-1) contains supplementary material, which is available to authorized users.

✉ Kun Luo
luokun@cczu.edu.cn

[1] School of Materials Science & Engineering, Changzhou University, Changzhou 213164, People's Republic of China

[2] School of Materials Science and Engineering, Baise University, Baise 533000, People's Republic of China

[3] College of Materials Science and Engineering, Guilin University of Technology, Guilin 541004, People's Republic of China

[4] Faculty of Pharmacy, University of Sydney, Sydney, NSW 2006, Australia

noticed that the Au NPs modified with tris(hydroxymethyl)phosphine oxide and triphenylphosphine at the toluene/water interface could be entirely replaced by dodecanethiol or mercaptoundecanoic acid, resulted in the Au-NP suspensions in toluene or water due to the stronger binding force of Au-S than that of Au-P [18, 19]. Recently, Vilian et al. found that the substitution of phosphinine with thiolate could be limited to some extent and Janus Au NPs with both thiolate and phosphinine domains were obtained by precisely control over the phosphinine/thiolate ratio in THF solution, demonstrating the feasibility of partly ligand exchange [17]. Herein, we present a facile approach to synthesize amphiphilic Janus Au NPs with compartmentalized thiolate and phosphine faces in batch, where partly ligand substitution of precursor Au NPs with triphenylphosphine (PPh_3) by D-penicillamine (D-PA) can be performed at the toluene/water emulsion interface.

Experimental

Materials and chemicals

Chloroauric acid hydrate ($HAuCl_4$, 99%, Shanghai Titan Scientific Co. Ltd., China), triphenylphosphine (PPh_3, > 99%, Aladdin Industrial Corporation, China), D-penicillamine (D-PA, ≥ 98%, Adamas Reagent Co., Ltd., China), N, N-dimethylformamide (DMF, ≥ 99.5%, Xilong Scientific Co., Ltd., China), toluene (≥ 99.5%, Xilong Scientific Co., Ltd., China), sodium hydroxide (NaOH, ≥ 96%, Xilong Scientific Co., Ltd., China), sodium borohydride ($NaBH_4$, ≥ 98%, Sinopharm Chemical Reagent Co., Ltd., China), and 4-nitrophenol (≥ 99%, Sinopharm Chemical Reagent Co., Ltd., China) were used directly without further treatment. Dichloromethane-d2 (CCl_2D_2, 99.5 at.% D) and trifluoroacetic acid-d (CF_3COOD, 99.5 at.% D) were from Beijing Innochem Science & Technology Co., Ltd., China. Deionized water (18.2 MΩ cm, 25 °C) was employed to prepare the aqueous solutions in the experiments.

Synthesis of amphiphilic Janus Au NPs

Forty-five milliliters of 1.0 mM PPh_3 toluene solution and 25 mL of 14.4 mM NaOH solution were added in an Erlenmeyer flask, followed with the injection of 10 mL of 4.5 mM $HAuCl_4$ into the aqueous phase. The mixture was agitated with an emulsifying mixer at a rate of 4000 rpm for 5 min, and then 5 mL of $NaBH_4$ solution (containing 17.0 mg $NaBH_4$) were added, where the reaction with $HAuCl_4$ was kept for 1.5 h, resulted in a dark brown colored suspension indicative of the formation of precursor Au NPs.

Five milliliters of 9.0 mM D-PA aqueous solution were injected into the Erlenmeyer flask with Au-NP toluene suspension and were mixed with an emulsifying mixer at a rate of 4000 r/min for 30 min to trigger ligand exchange. The emulsion was moved in a separating funnel and left overnight, resulting in the separation of water and toluene phases. The reaction product at the toluene/water interface was removed and rinsed with a mixed solvent of toluene and deionized water (at the volume ratio of 1:1) for three times by centrifuging at 10000 rpm. After freeze-drying, the amphiphilic Janus Au NPs were obtained.

Characterizations

A transmission electron microscope (TEM, JEM-2100F, JEOL, operated at 200 kV) and an X-ray diffractometer (Smartlab 9 kW, Rigaku, operated at 40 kV with Cu Kα radiation) were used to characterize the morphology and crystalline structure of the core Au NPs in the product, and the crystal size was evaluated by the Debye-Scherrer's method. The surface chemistry of the product was studied by nuclear magnetic resonance spectroscopy (^{1}H NMR, Bruker AV-400, Germany), Fourier transform infrared spectroscopy (FTIR, IRTracer- 100, Shimadzu), Raman spectroscopy (DXR, Thermo Fisher Scientific, with a laser beam at 532 nm), and X-ray photoelectron spectroscopy (XPS, ESCALAB 250Xi, Thermo Fisher Scientific).

The ratio of thiolate to phosphine ligands (C_A) was estimated from the XPS analysis by the Scofield sensitivity factor as follows:

$$N_A = S_A / SF_{\text{Scofield}} \times TF \times KE^{0.6} \quad (1)$$

$$C_A(at\%) = \frac{N_A}{\sum_i N_i} \times 100 \quad (2)$$

where N_A is the normalized area of spectral peak, S_A is the fitting peak area, $SF_{Scofield}$ is the sensitivity factor, TF is the transfer function, and KE is the electronic kinetic energy.

Nuclear Overhauser enhanced spectroscopy (NOESY) was used to analyze the phase segregation of capping molecules on the Au NPs. NOESY is a two-dimensional phase-sensitive NMR technique that detects the distance-dependent nuclear Overhauser effect between proton spins of the sample [20, 21]. In this experiment, 30 mg of the product were dispersed in a mixture (0.6 mL) of dichloromethane-d2 and trifluoroacetic acid-d (at a volume ratio of 1:1) by ultrasonic stirring, and an NMR instrument (Bruker AV-400, Germany) was used to carry out the NOESY analysis of the sample.

The phase separation of capping ligands on the Au NPs was also examined by the wetting discrepancy on the two faces of the Langmuir reassemblies of the as-dispersed product, according to our previous work [16]. In the experiment, 1.0 mg of the product was firstly dispersed in 10 mL DMF by ultrasonic stirring. A double beam UV-vis spectrophotometer (TU-1901, Beijing Purkinje General Instrument Co., Ltd.)

was used to differentiate the dispersed and assembled states of the product by the feature of surface plasmon resonance (SPR). Then, 9 mL of the colloid were employed to spread on the water surface in a Langmuir trough (JML04C1-P, 210 mm × 80 mm × 8 mm, Shanghai Zhongchen Digital Technical Apparatus Co., Ltd., China), and the Langmuir film composed of the reassembled Au NPs was prepared by compression at 12 mN m^{-1}, which was collected by a clean glass slide (1 mm × 12 mm × 60 mm).

Two ways to collect the Langmuir reassemblies of the dispersed product were used. The Langmuir film was lifted up by the upstroke movement of a slide underneath the film, led to the lipophilic side out (surface A) by folding over across the slide. As the slide pressed downwards into the water, the film was flipped over and let the hydrophilic side out (surface B). The wettability of the collected Langmuir reassemblies was examined by a contact angle analyzer (JGW-360A, Xiamen Chongda Intelligent Technology Co., Ltd., China).

The catalytic performance of the amphiphilic Janus Au NPs was tested by the reduction of 4-nitrophenol, where 0.2 mL of 2 mM 4-notrophenol aqueous solution and 2.2 mL deionized water were added into a quartz cuvette, followed with the addition of 1.2 mL of 40 mM $NaBH_4$. Then, 0.4 mL of 0.2 mg mL^{-1} amphiphilic Janus Au NPs suspension was added and allowed to react under ultrasonic stirring. Time-dependent changes of UV-vis absorbance at 399 nm were recorded to monitor the reduction process with and without the presence of Au NPs.

Results and discussion

Morphology and structure of the product

Figure 1 a displays the TEM image of the product, where the average diameter of the Au NPs is measured as 3.7 ± 0.6 nm (N = 322) in the upper inset. The lattice space of the Au nanoparticle is gauged as 0.24 nm shown in the HRTEM image in Fig. 1b, corresponding to the Au (111) plane in line with the previous literature [22]. Especially, the Au NPs are seen to aggregate in form of small vesicles in size of about 30 nm as illustrated in Fig. 1c, suggestive of the association with the toluene/water emulsion drops during ligand exchange reaction. Figure 1 d shows the XRD diffractions of the product, which appear at 38.26°, 44.35°, 64.78°, 77.56°, and 81.74° assigned to the (111), (200), (220), (311), and (222) lattice planes of Au crystal (PDF#04-0784), respectively. The broadening of the diffraction peaks is attributed to ultrafine Au NPs in the product, and the crystal size can be estimated by Debye-Scherrer formula:

$$D = K\lambda/\beta cos\theta \quad (3)$$

where K is the Scherrer's constant, λ is the X-ray wavelength (Cu k_α = 0.1541 nm), β is the full width at half maximum (*FWHM*) of diffraction peak, and θ is the Bragg angle. The calculated crystallite size is 4.1 nm, close to the particle size of Au NPs shown in Fig.1a, indicating that the Au NPs are actually nanocrystals.

Surface chemistry of the product

The product was characterized by XPS analysis, where Fig. S1 displays the total survey spectrum in the Supporting Information, indicative of the existence of C, O, Au, N, P, and S elements. The fitting of the resolved Au_{4f} signal (Fig. 2a) manifests two major peaks at 83.9 eV and 87.6 eV, assigned to the $Au_{4f7/2}$ and $Au_{4f5/2}$ of metallic Au, respectively. Figure 2 b shows two fitted peaks for the resolved P_{2p} signal at 131.2 eV and 132.0 eV, in correspondence to the $P_{2p3/2}$ and $P_{2p1/2}$. The fitting of the S_{2p} peak ends up with two peaks at 162.0 eV and 163.2 eV as displayed in Fig. 2c, attributed to the $S_{2p3/2}$ and $S_{2p1/2}$. The fitting of the N_{1s} signal results in just one peak at 400.2 eV as plotted in Fig. 2d. The C_{1s} signal is fitted with three peaks at 284.8 eV, 285.7 eV, and 290.4 eV as depicted in Fig. 2e, assigned to the C-C, C-S (and C-N) and -COOH groups. As for the fitting of O_{1s} signal in Fig. 2f, two peaks are observed at 532.3 eV and 533.4 eV, indicative of the -COOH and O-H groups, respectively. The above results are listed in Table 1, from which the molecular ratio of the hydrophilic molecule (D-PA) to the lipophilic ligand (PPh_3) is estimated at about 1.85 based on the atomic ratio of S to P (S/P).

Figure 3 a displays the FTIR spectrum of the product, where the broad band at 3421 cm^{-1} is attributed to the O-H stretch, and the peak at 3049 cm^{-1} can be assigned to = C-H stretch in aromatics. The bands at 2922 cm^{-1} and 2853 cm^{-1} represent the -CH_3 anti-symmetric and symmetric stretching in aliphatic chains, respectively. The peak at 1689 cm^{-1} is attributed to the C=O stretch in carboxylic acids, and the one at 1650 cm^{-1} is likely originated from the -NH_2 deformation in primary amines. The bands at 1552 cm^{-1} and 1361 cm^{-1} are assigned to the COO^- group anti-symmetric and symmetric stretching, respectively. The band at 1517 cm^{-1} is probably attributed to the C=C stretch in benzene ring, and the absorbance at 1425 cm^{-1} corresponds to the C-P group stretching.

Figure 3 b shows the Raman spectrum of the product. The band at 1562 cm^{-1} represents the C=C stretch in aromatic compounds, and the peak at 1423 cm^{-1} is attributed to the C-P group stretching. The two bands at 1260 cm^{-1} and 1308 cm^{-1} represent the -CH_3 deformation, and the peak at 1175 cm^{-1} is assigned to the -CH_3 rocking. The band at 1090 cm^{-1} presents the C-N stretching, and the peak at 842 cm^{-1} is probably originated from the C-C-N symmetric stretching mode. The bands at 1028 cm^{-1} and 989 cm^{-1} can be assigned to the C-H in-plane bending and ring breathing in

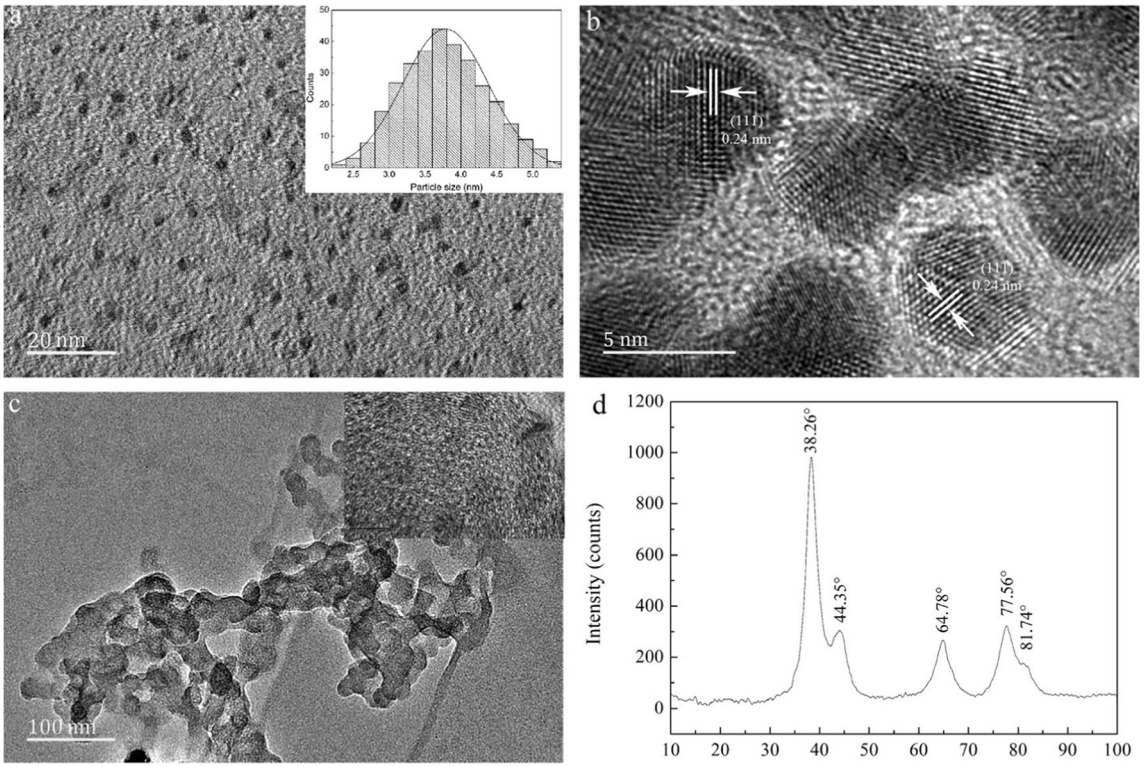

Fig. 1 TEM image of the product (**a**), HRTEM image of Au cores (**b**), vesicular assembly structure (**c**), and XRD pattern of the product (**d**)

aromatic compounds, respectively, and the two peaks at 728 cm^{-1} to 695 cm^{-1} can be assigned to the C-H out-of-plane deformation. The band at 521 cm^{-1} can be assigned to the C-S stretch in mercaptans. The peak at 407 cm^{-1} is attributed to C-C=O bend in carboxylic acid, and the band at 279 cm^{-1} represents the -C-C-C- bending. Both the FTIR and Raman results suggest the presence of D-PA and PPh_3 molecules on the Au NPs in the product.

The capping molecules were also analyzed by using ^1H NMR spectroscopy according to the chemical shifts of protons, where quantitative analysis could be carried out by the integral area of the peaks in the spectrum. In Fig. 3c, the chemical shifts of protons at 11.17 ppm and 5.32 ppm are attributed to the residual solvents of trifluoroacetic acid-d (including water) and dichloromethane-d2, respectively. The peaks at 7.65 ppm and 7.23 ppm are assigned to the protons in the benzene rings of PPh_3 molecule, and the ones at 1.68 ppm and 2.37 ppm correspond to the protons of methyl ($-CH_3$) and methine (-CH) groups in D-PA molecule. Comparing the integral peak area at 1.68 ppm to the sum at 7.65 ppm and 7.23 ppm, the ratio of D-PA to PPh_3 (S/P) is estimated as 1.75 in agreement with the XPS analysis.

The distribution of capping ligands on the Au NPs of the product was determined by NOESY technique [20, 23, 24], which is a two-dimensional phase-sensitive NMR analysis based on the distance-dependent nuclear Overhauser effect between proton spins [21]. It is clear that all the resonances in the spectrum are well aligned along the diagonal direction as shown in Fig.3d, demonstrating that the hydrophilic (D-PA) and lipophilic (PPh_3) ligands are segregated on two compartments of the Au NP's surface. In other words, the Au NPs in the product are amphiphilic Janus nanoparticles modified with two distinct faces of D-PA and PPh_3 molecules.

The amphiphilic feature of the Au NPs in the product was also examined by the wettability of Langmuir reassemblies. In the experiment, the product was firstly dispersed in DMF by ultrasonic stirring. Then, the as-dispersed individual Au NPs in DMF were spread on water surface, which were reassembled in the form of Langmuir films after compression. Figure 4 a shows a band at 535 nm in the UV-vis spectrum of the dispersed product in DMF, while the Langmuir film presents a peak at 578 nm. The red shift of the Langmuir film is attributed to the supramolecular interaction among the Au NPs, which indicates the self-assembled Au NPs. Figure 4 b displays the isotherm of Langmuir compression, where the assembly of the floating Au NPs appears in the form of gaseous (G), liquid (L) and solid (S) states with the increase of pressure. Based on the result, the Langmuir film was prepared at the compression of 12 mN m^{-1}.

The wetting difference on the two faces of the Langmuir reassembly therefore reflects the amphiphilicity of the individual Au NPs in the as-synthesized product. The inserted picture in Fig. 4b shows the ways of collecting the Langmuir films by the upstroke and downstroke movements of the glass slides, by which the contact angles on the two faces were available to be measured. The contact angles of a water drop on the surface

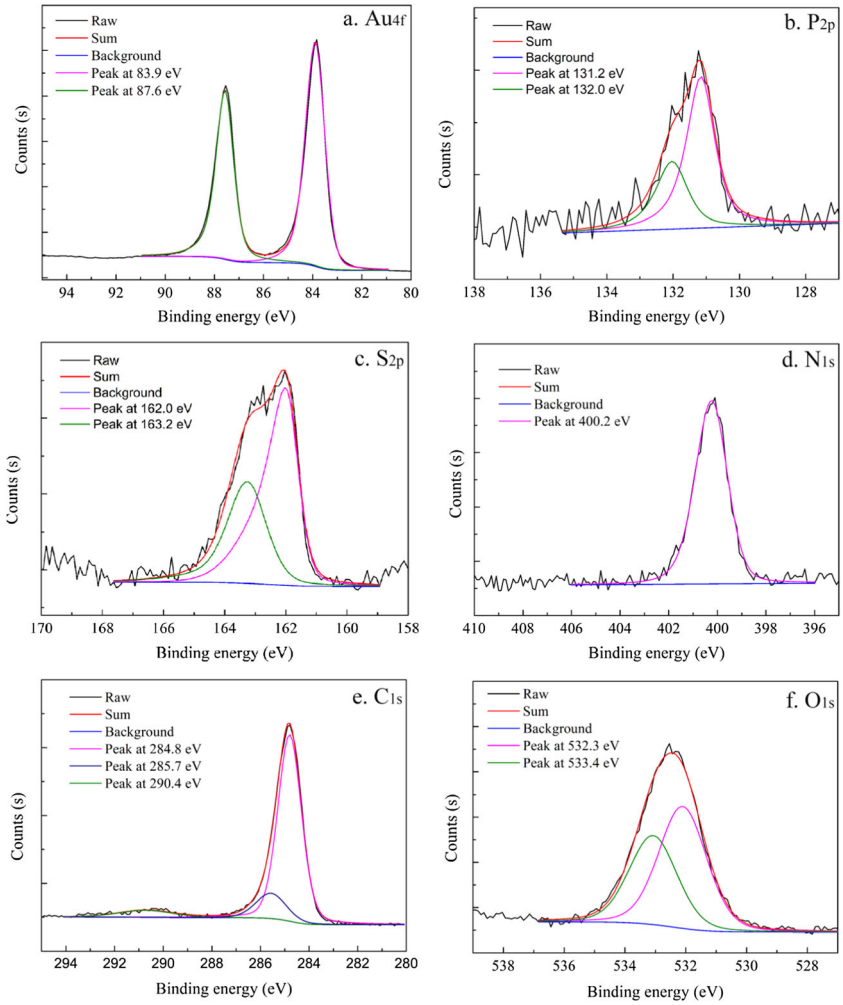

Fig. 2 XPS analysis of the product

A (lipophilic side out) and surface B (hydrophilic side out) were measured as 77.5° and 30.3°, respectively, verifying that the phase separation of the PPh_3 and D-PA ligands occurs on the individual Au NPs in the product, in agreement with the NOESY analysis.

Table 1 XPS analysis of the product

Elements	B.E. (eV)	Possible chemistry	Atomic percentage (%)
Au_{4f}	83.9	$Au_{4f7/2}$	17.28
	87.6	$Au_{4f5/2}$	
P_{2p}	131.2	$P_{2p3/2}$	2.09
	132.0	$P_{2p1/2}$	
S_{2p}	162.0	$S_{2p3/2}$	3.86
	163.2	$S_{2p1/2}$	
N_{1s}	400.2	C-N	3.47
C_{1s}	284.8	C-C	47.80
	285.7	C-S, C-N	8.30
	290.4	-COOH	4.13
O_{1s}	532.3	-COOH	7.56
	533.4	-OH	5.51

Competitive ligand adsorption on Au NPs

Figure 5 a is a schematic diagram that shows the formation of Janus Au NPs via ligand exchange reaction at toluene/water interface, during which a portion of the PPh_3 ligand on the precursor homogenous Au NPs is replaced by D-PA molecule, leading to the amphiphilic Janus Au NPs with two phosphine and thiolate faces. The formation of Janus Au NPs was a rapid kinetic process. The inset of Fig. 5b directly shows the ligand exchange process by the color change in toluene phase: (1) Before ligand exchange reaction, the precursor Au NPs stabilized with PPh_3 are steadily suspended in toluene, which appears in a color of brown black; (2) 8 min later, a majority of the Au NPs in toluene moved to the toluene/water interface in form of aggregates, accompanied with the color fading in the toluene solution; and (3) after 15 min of reaction, nearly all Au NPs were enriched at the toluene/water interface, and both the toluene and aqueous phases were colorless. The ligand

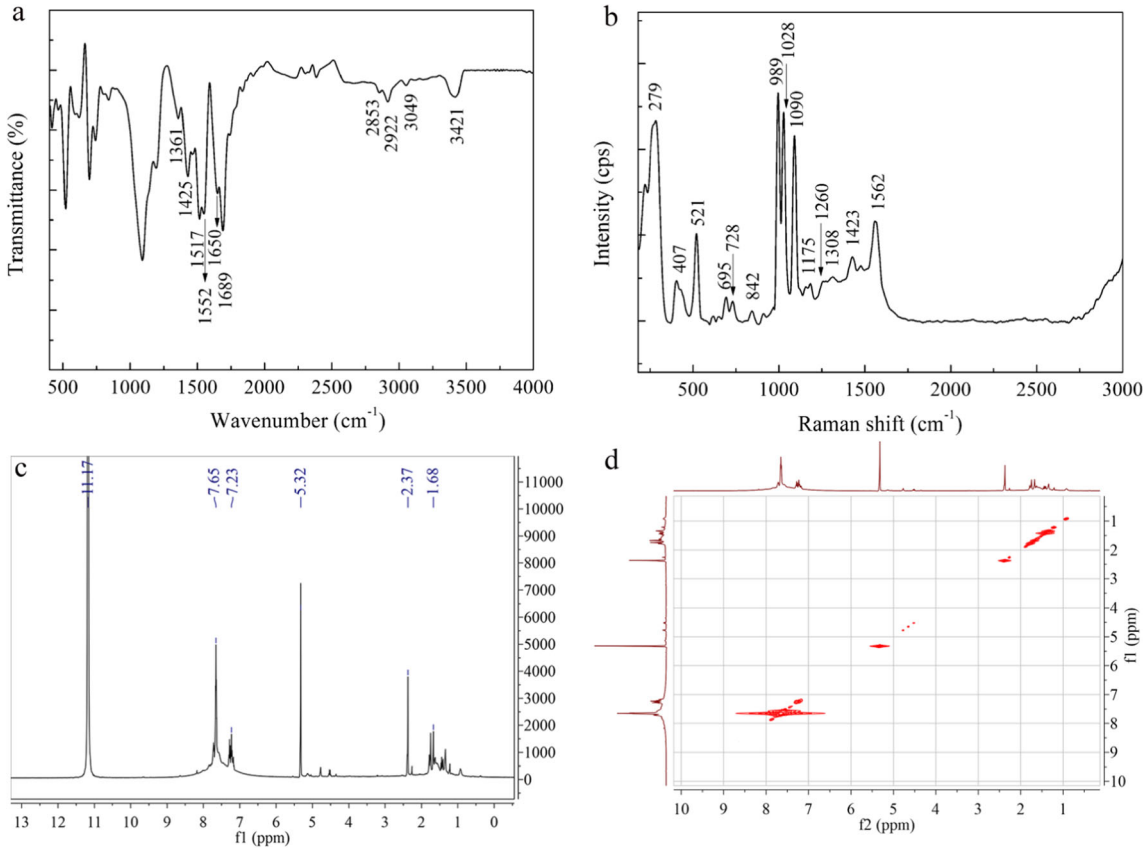

Fig. 3 FTIR (**a**), Raman (**b**), ^{1}H NMR (**c**), and NOESY (**d**) analyses of the product

exchange process was also assessed by the S/P ratio (i.e., D-PA to PPh_3) sampled at variant reaction periods by XPS analysis. Figure 5 b shows the curve of the S/P ratio in the product with reaction time, which sharply increases in the first 15 min, indicative of the quick substitution of PPh_3 by D-PA on the Au NPs. Afterwards, the curve reaches a plateau that extends up to 240 min, suggesting the equilibrium of ligand exchange.

Moreover, the process can be also investigated by UV-vis absorbance at λ_{max} = 539 nm in toluene at different lengths of reaction. As illustrated in Fig. 5c, the absorbance of the Au

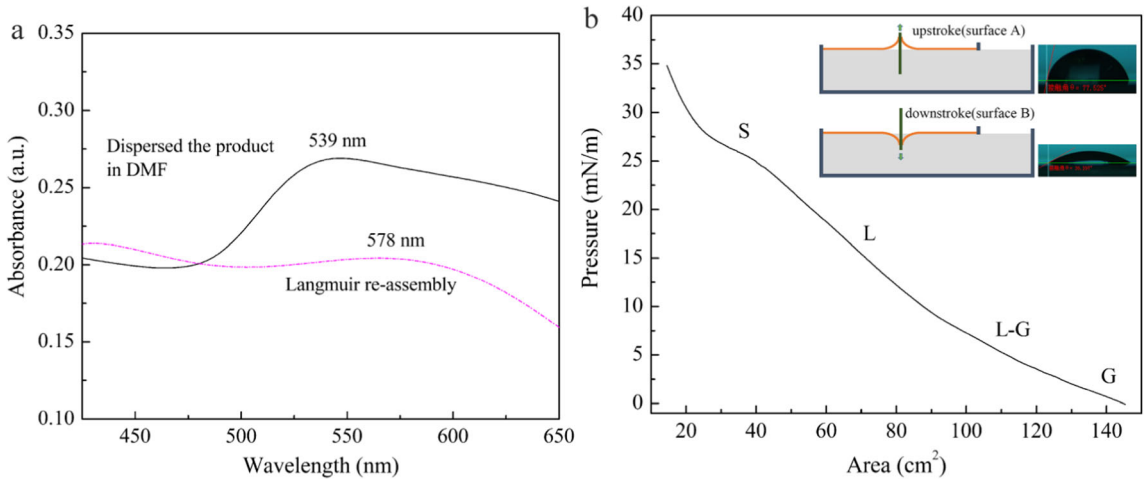

Fig. 4 Characterizing the phase separation of the Au NPs through Langmuir reassembly of the dispersed product. UV-vis spectra of the product dispersed in DMF and Langmuir reassembly (**a**) and compression isotherm and the contact angles on the two faces of the reassemblies (inset) (**b**)

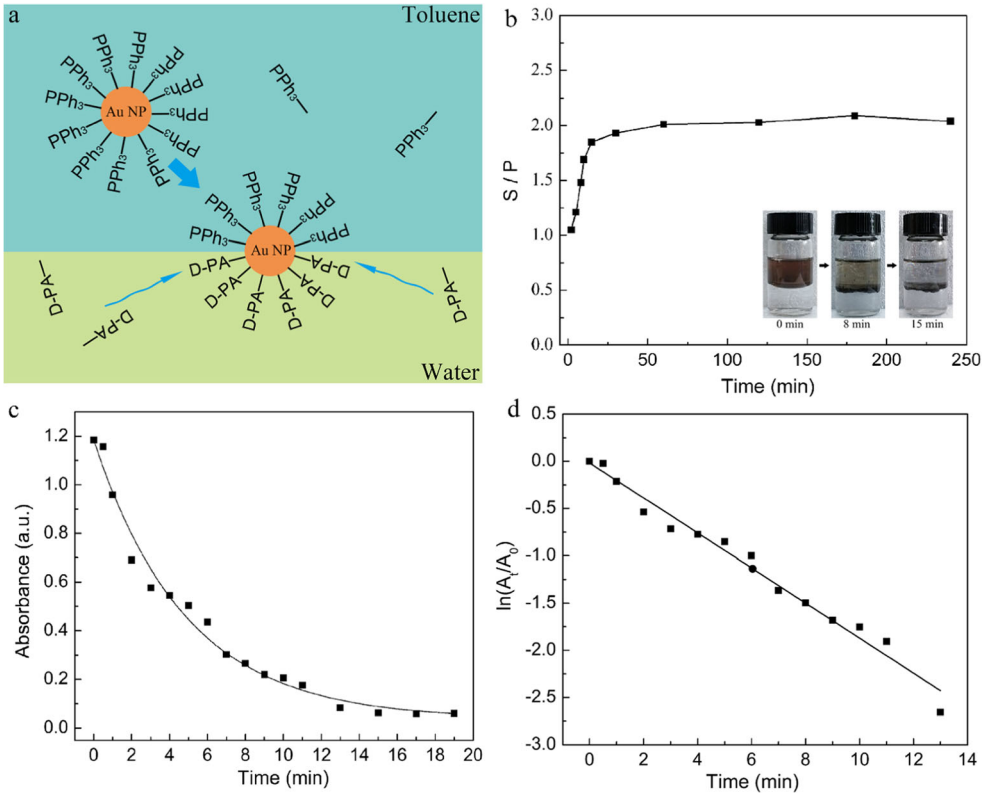

Fig. 5 Schematic illustration of PPh_3 partially replaced by D-PA at toluene/water interface (**a**), the variation of S/P with reaction time (**b**), the variation of UV-vis absorbance at $\lambda_{max} = 535$ nm with reaction time (**c**), and the relationship of $ln(A_t/A_0)$ of toluene phase versus reaction time (**d**)

NPs in toluene declines quickly within the initial 15 min, and only less than 10% of intensity is remained afterwards. The kinetics of the ligand exchange reaction can be further estimated by the absorbance variation according to the following equation:

$$In(C_t/C_0) = \mathrm{In}(A_t/A_0) = -K_{app}t \quad (4)$$

where the C_t and A_t represent the content of Au NPs in toluene and the corresponding absorbance at the time t, the C_0 and A_0 the content of Au NPs in toluene and the corresponding absorbance before ligand exchange ($t = 0$), and K_{app} is the apparent rate constant of ligand exchange reaction. Figure 5 d displays a linear relationship of $\ln(A_t/A_0)$ versus reaction time, suggestive of the first order reaction. The apparent rate constant K_{app} was estimated as 0.19 min^{-1} at room temperature from the gradient of the fitting line.

It is accepted that the binding force of Au-S is stronger than that of Au-P, which enables the ligand substitution of phosphine by thiolate molecules on the surface of Au NPs. However, this experiment suggests that the rapid ligand substitution of PPh_3 with D-PA stops in midway, leading to the formation of amphiphilic Janus Au NPs with phosphine and thiolate faces. Figure S3 displays that the color of water phase turns pink (indicative of some hydrophilic Au NPs) as total ligand substitution of PPh_3 by D-PA was commenced under slow stirring for 24 h reaction, demonstrating the connection of amphiphilic Janus Au NPs with the toluene/water emulsion system. XPS analysis further indicates in Fig. S2 and Table S1 that the amphiphilic Janus Au NPs are stable enough to stand the attack of D-PA, where the S/P ratio is not changed when the as-synthesized product was again dispersed in 1 mM D-PA solution under magnetic stirring for 2 h. The mechanic investigation on the ligand exchange at emulsion interfaces is still underway.

As a potential heterogeneous catalyst, the preliminary use of amphiphilic Janus Au NPs on the reduction of 4-nitrophenol (4-NP) to 4-aminophenol (4-AP) by excess amount of $NaBH_4$ (in the molar ratio of $NaBH_4$ to 4-NP of 120:1) was commenced, where the time-dependent variation of absorbance was monitored by UV-vis spectroscopy at the wavelength of 399 nm (the characteristic peak of 4-NP) [25]. It was observed that there was no visible change on the absorbance after 30 min in the absence of the amphiphilic Janus Au NPs, indicating that no reaction happened. However, when the suspension of amphiphilic Janus Au NPs (shown in the left photo of Fig. S4a) was added, the absorbance began to decrease after a probation period (Fig. S4b), where the fitting line of $\ln(A_t/A_0)$ versus reaction time is linear (Fig. S4c), suggestive of the first order kinetics with the apparent rate constant K_{app} of 0.12 min^{-1} [26]. Different from hydrophilic Au NPs, the amphiphilic Janus Au NPs can be easily separated from the solution by magnetic stirring with toluene, where the

amphiphilic Janus Au NPs are enriched at the toluene/water interface (see the right image of Fig. S4a), available for catalysis again after rinsing with the toluene/water mixture (at the volume ratio of 1:1).

Conclusion

Amphiphilic Janus Au NPs coated with compartmentalized D-PA and PPh_3 faces were synthesized by a fast ligand exchange reaction at toluene/water emulsion interface. TEM and XRD analyses indicate that the product is composed of Au nanocrystals in an average diameter of about 3.7 nm. XPS, FTIR, Raman, and ^1H NMR analyses demonstrate that the Au NPs in the product are modified with D-PA and PPh_3 at the S/P ratio of around 1.8. The NOESY analysis and contact angle measurement further suggest that the D-PA and PPh_3 molecules are separated into the hydrophilic and lipophilic compartments on the individual Au NPs. The amphiphilic Janus Au NPs exhibit good catalytic performance on the reduction of 4-nitrophenol and can be easily separated and reused due to their amphiphilic nature. The simple approach allows the batch synthesis of amphiphilic Janus Au NPs with compartmentalized thiolate and phosphine faces at low cost, which is potentially applicable for other phosphine/thiolate pairs to modify Au NPs.

Funding information The authors gratefully acknowledge the support from the National Natural Science Foundation of China (No. 51874051 and 21163004) and Guangxi Natural Science Foundation (No. 2018GXNSFAA138133).

References

1. Gennes PGD (1992) Soft matter (Nobel Lecture) [J]. Angew Chem Int Ed 31(7):842–845
2. Luo K, Xiang Y, Wang H, Xiang L, Luo Z (2016) Multiple-sized amphiphilic Janus gold nanoparticles by ligand exchange at toluene/water interface [J]. J Mater Sci Technol 32(8):733–737
3. Zhao P, Li N, Astruc D (2013) State of the art in gold nanoparticle synthesis [J]. Coord Chem Rev 257:638–665
4. Jackson AM, Hu Y, Silva PJ, Stellacci F (2006) From homoligand- to mixed-ligand-monolayer-protected metal nanoparticles: a scanning tunneling microscopy investigation [J]. J Am Chem Soc 128(34):11135–11149
5. Hashmi ASK, Hutchings GJ (2006) Gold catalysis [J]. Angew Chem Int Ed 45(47):7896–7936
6. Hashmi ASK (2007) Gold-catalyzed organic reactions [J]. Chem Rev 107(7):3180–3211
7. Crossley S, Faria J, Shen M, Resasco DE (2010) Solid nanoparticles that catalyze biofuel upgrade reactions at the water/oil interface [J]. Science 327(5961):68–72
8. Cole-Hamilton DJ (2010) Janus catalysts direct nanoparticle reactivity [J]. Science 327(5961):41–42
9. Luo K, Huang T, Luo Y, Wang H, Sang C, Li X (2013) Thin film assembly of gold nanoparticles for vapor sensing via droplet interfacial reaction [J]. J Mater Sci Technol 29(5):401–405
10. Glogowski E, He J, Russell TP, Emrick T (2005) Mixed monolayer coverage on gold nanoparticles for interfacial stabilization of immiscible fluids [J]. Chem Commun 32(32):4050–4052
11. Nørgaard K, Weygand MJ, Kjaer K, Brust M, Bjørnholm T (2004) Adaptive chemistry of bifunctional gold nanoparticles at the air/water interface. A synchrotron X-ray study of giant amphiphiles [J]. Faraday Discuss 125(125):221–233
12. Luo K, Wang H, Li X (2014) Electrocatalytic activity of ligand-protected gold particles: formaldehyde oxidation [J]. Gold Bull 47(1–2):41–46
13. Cao H, Yang Y, Chen X, Zhao Z (2016) Intelligent Janus nanoparticles for intracellular real-time monitoring of dual drug release [J]. Nanoscale 8(12):6754–6760
14. Binder WH (2005) Supramolecular assembly of nanoparticles at liquid-liquid interfaces [J]. Angew Chem Int Ed 44(33):5172–5175
15. Pradhan S, Xu L, Chen S (2007) Janus nanoparticles by interfacial engineering [J]. Adv Funct Mater 17(14):2385–2392
16. Luo K, Hu C, Luo Y, Li D, Xiang Y, Mu Y, Wang H, Luo Z (2017) One-pot synthesis of ultrafine amphiphilic Janus gold nanoparticles by toluene/water emulsion reaction [J]. RSC Adv 7(81):51605–51611
17. Vilain C, Goettmann F, Moores A, Floch PL, Sanchez C (2007) Study of metal nanoparticles stabilised by mixed ligand shell: a striking blue shift of the surface-plasmon band evidencing the formation of Janus nanoparticles [J]. J Mater Chem 17(33):3509–3514
18. Rao CNR, Kulkarni GU, Agrawal VV, Gautam UK, Ghosh M, Tumkurkar U (2005) Use of the liquid–liquid interface for generating ultrathin nanocrystalline films of metals, chalcogenides, and oxides [J]. J Colloid Interface Sci 289(2):305–318
19. Luo K, Schroeder SLM, Dryfe RAW (2009) Formation of gold nanocrystalline films at the liquid/liquid interface: comparison of direct interfacial reaction and interfacial assembly [J]. Chem Mater 21(18):4172–4183
20. Pradhan S, Brown LE, Konopelski JP, Chen S (2009) Janus nanoparticles: reaction dynamics and NOESY characterization [J]. J Nanopart Res 11(8):1895–1903
21. Morris KF, Froberg AL, Becker BA, Almeida VK, Tarus J, Larive CK (2005) Using NMR to develop insights into electrokinetic chromatography [J]. Anal Chem 77(13):255–263
22. Kemal L, Jiang XC, Wong K, Yu AB (2008) Experiment and theoretical study of poly (vinyl pyrrolidone)-controlled gold nanoparticles [J]. J Phys Chem C 112(40):15656–15664
23. Liu X, Yu M, Kim H, Mameli M, Stellacci F (2012) Determination of monolayer-protected gold nanoparticle ligand-shell morphology using NMR [J]. Nat Commun 3(6):1182–1190
24. Hyewon K, Carney RP, Javier R, Ong QK, Liu X, Francesco S (2012) Synthesis and characterization of Janus gold nanoparticles [J]. Adv Mater 24(28):3857–3863
25. Du X, He J, Zhu J, Sun L, An S (2012) Ag-deposited silica-coated Fe_3O_4 magnetic nanoparticles catalyzed reduction of p-nitrophenol [J]. Appl Surf Sci 258(7):2717–2723
26. Wang M, Niu R, Huang M, Zhang Y (2015) The surface structural changes of self-assembly monolayer au nanoparticles and their regulated catalytic activity [J]. Sci Sin Chim 45(1):76–89